Aerodynamic size-resolved composition and cloud condensation nuclei properties of aerosols in Beijing suburban region

Chenjie Yu[1,2], Dantong Liu[1], Kang Hu[1], Ping Tian[3], Yangzhou Wu[1], Delong Zhao[3], Huihui Wu[2], Dawei Hu[2], Wenbo Guo[2], Qiang Li[4], Mengyu Huang[3], Deping Ding[3] and James D. Allan[2,5]

[1] Department of Atmospheric Sciences, School of Earth Sciences, Zhejiang University, Zhejiang 310027, China

[2] Department of Earth and Environmental Sciences, University of Manchester, Manchester M13 9PL, United Kingdom

[3] Beijing Weather Modification Office, Beijing 100089, China

[4] Cambustion Ltd China Office, Shanghai 201112, China

[5] National Centre for Atmospheric Sciences, University of Manchester, Manchester M13 9PL, United Kingdom

Correspondence to: Dantong Liu (dantongliu@zju.edu.cn) and James Allan (james.allan@manchester.ac.uk)

Abstract The size-resolved physiochemical properties of aerosols determine their atmospheric lifetime, cloud interactions, and the deposition rate on human respiratory system, however most atmospheric composition studies tend to evaluate these properties in bulk. This study investigated size-resolved constituents of aerosols on mass and number basis, and their droplet activation properties, by coupling a suite of online measurements with an aerosol aerodynamic classifier (AAC) based on aerodynamic diameter (D_a) in Pinggu, a suburb of Beijing. While organic matter accounted for a large fraction of mass, a higher contribution of particulate nitrate at larger sizes (D_a > 300 nm) was found under polluted cases. By considering the mixing state of refractory black carbon containing particles (rBCc) and composition-dependent densities, aerosols including rBCc were confirmed nearly spherical at D_a > 300 nm. Importantly, the number fraction of rBCc was found to increase with D_a at all pollution levels. The number fraction of rBC is found to increase from ~3% at ~90 nm to ~15% at ~1000 nm, and this increasing rBC number fraction may be caused by the coagulation during atmospheric aging. The droplet activation diameter at a water supersaturation of 0.2% was 112 ± 6 nm and 193 ± 41 nm for all particles with D_a smaller than 1 μm (PM_1) and rBCc respectively. As high as 52 ± 6% of rBCc and 50 ± 4% of all PM_1 particles in number could be activated under heavy pollution due to enlarged particle size, which could be predicted by applying the volume-mixing of substance hygroscopicity within rBCc. As rBCc contributes to the quantity of aerosols at larger particle size, these thickly coated rBC may contribute to the radiation absorption significantly or act as an important source of cloud condensation nuclei (CCN). This size regime may also exert important health effects due to their higher deposition rate.

1. Introduction

Atmospheric aerosols make a significant contribution in a number of atmospheric chemical and physical processes (Riemer et al., 2019). Aerosols from anthropogenic emissions have negative impact on air quality and human health (West et al., 2016). As a major megacity, the air pollution in Beijing and its surrounding regions has raised much attention in the past years (Shi et al., 2019). The rapid urbanization and the continued increase in vehicle numbers have contributed to a complicated air pollution situation in Beijing (Squires et al., 2020). A number of in-situ measurements have

characterised the submicron aerosol compositions in urban Beijing (Wang et al., 2020; Hu et al., 2016; Wang et al., 2019). However, few studies have characterised the detailed composition or cloud condensation nuclei (CCN) abilities of particles at Beijing rural sites (Chen et al., 2020a). The relocation of industry from the urban Beijing has led the surrounding cities around Beijing to be highly industrialised in recent years (Wang et al., 2018), and the rural sites of Beijing are significantly impacted by the air pollutants transported from the surrounding industrial regions in North China Plain (NCP) (Wu et al., 2011). Furthermore, controls targeting pollution from residential solid fuel use and diesel vehicles do not apply outside of the main metropolitan area of Beijing. The detailed characterisation of fine aerosol physiochemical properties in a variety of different environments is essential to understand the evolution of atmospheric particulate matter.

Fine particulate matter can also cause damage to human health via the respiratory system (Xing et al., 2016;Xu et al., 2016). The aerodynamic size of aerosols crucially determines the area of deposition (Sturm, 2010;Vu et al., 2018;Sturm, 2017), e.g. particles with an aerodynamic diameter (D_a) below 2.5 μm can reach the alveoli in the lungs and possibly pass into the blood (Lipworth et al., 2014). Through particle-resolving model simulation, Ching and Kajino (2018) found that the deposition efficiency in human alveoli also depended on the mixing state. The toxicity of aerosols is composition dependent (Kwon et al., 2020) and influenced by the complex morphology (Sturm, 2010; Vu et al., 2018), therefore the aerodynamic size-resolved properties of aerosols are important when understanding their influences on human health.

Atmospheric aerosols also play important roles in climate through scattering and absorbing solar radiation directly, or indirectly through altering cloud properties (Liu et al., 2020; Ravishankara et al., 2015) or causing snow melt after deposition. Black carbon (BC) is produced from incomplete combustion and is the dominant optically absorbing component in aerosols (Liu et al., 2020; Bond et al., 2013). By mixing with other compounds, the absorption ability of coated BC can be enhanced through the "lensing effect" (Lack and Cappa, 2010). However, detailed simulation and characterization of optical properties of BC remains uncertain since it is influenced by

93 factors such as shape and mixing state (Cappa et al., 2012; Liu et al., 2017; Fierce et
94 al., 2020), which can be modified through atmospheric processing. Thus, better
95 characterization of light absorbing carbonaceous particles is essential.
96

97 Coated BC is also known as an important form of CCN and wet removal is its main
98 atmospheric loss mechanism, so its in-cloud scavenging efficiency and thus lifetime is
99 influenced by its size, mixing state and hygroscopic properties (Taylor et al., 2014), but
100 this is subject to large uncertainties (Myhre and Samset, 2015). Studies have confirmed
101 that the hygroscopicity of rBCc is largely dictated by the coating material, and rBCc
102 will transform from hydrophobic to hydrophilic after emission by acquiring more non-
103 BC material and increasing in size (Hu et al., 2020a; Wu et al., 2019; Liu et al., 2013).
104 Previous studies (Levin et al., 2014; Broekhuizen et al., 2006; Gunthe et al., 2011; Fan
105 et al., 2020; Wu et al., 2017) have provided both the measured size-resolved CCN
106 ability and aerosol physiochemical properties. However, the CCN ability of rBCc based
107 on atmospheric data remains poorly constrained. Previously, size-resolved composition
108 has been widely investigated using size-segregated off-line analysis of cascade
109 impactor samples (Marple et al., 1991). This technique offers great advantages in
110 obtaining detailed information about composition in combination with advanced offline
111 measurements, however it often requires large amounts of material and may not be able
112 to provide sufficient time resolution. Information about particle mixing state and CCN
113 activity are also not available through this technique. The aerosol mass spectrometer
114 (AMS) is also capable of delivering size-resolved aerosol compositions, however the
115 poor accuracy of AMS in the size range important for CCN (typically 50 -100 nm) has
116 hampered quantitative work for the application of CCN concentration derivation based
117 on κ-Köhler theory (Petters and Kreidenweis, 2007).
118

119 A previous study (Yu et al., 2020) has characterized the size-resolved rBCc mixing
120 state in Beijing using a tandem aerosol classifier system. To explore the size-resolved
121 physiochemical properties and CCN ability for bulk aerosol compositions, here we
122 performed a new online measurement method by coupling an Aerodynamic Aerosol
123 Classifier (AAC) with different aerosol measurement techniques including a Single-
124 Particle Soot Photometer (SP2) and an Aerosol Mass Spectrometer (AMS). Comparing

to the previous studies performed with Differential Mobility Analyzer (DMA), the AAC classifies particles without multiple charging artefacts in a wide size range and with better transmission efficiency (Johnson et al., 2018). The simultaneous measurement of size-resolved chemical composition and CCN activation enables a detailed analysis of rBCc hygroscopicity and its size-dependent contribution to the CCN activation in a polluted environment. This information will deliver a better understanding to the BC deposition properties for the climate and air pollution impacts on human health studies.

2. Experimental methods

2.1 Experiment location and instruments

The experiment was performed between 5th Jan and 20th Jan 2020 in the Beijing Weather Modification Office field experiment base located in Pinggu (the red pentagram shown in Fig. 4a), a northeastern suburb of Beijing (Shi et al., 2019). With agriculture dominated its local economy, Pinggu is surrounded by small villages and farmlands (Han et al., 2020). Fig. 1 describes the schematic of the instruments used for the size-resolved aerosol measurements. An Aerodynamic Aerosol Classifier (AAC, Cambustion) was placed upstream of the aerosol measurement instruments. The operation and validation of the AAC was described in previous studies (Tavakoli and Olfert, 2013; Tavakoli and Olfert, 2014). Unlike the DMA or Centrifugal Particle Mass Analyzer (CPMA), the AAC selects particles based on aerodynamic sizes according to particle relaxation time without needing charging for electrostatic or mass sizing. A suite of online measurements was introduced downstream of the AAC, including a high-resolution time of flight aerosol mass spectrometer (HR-ToF-AMS, Aerodyne) (Decarlo et al., 2006), which was operated in V-mode to characterize the non-refractory aerosol composition, and a single particle soot photometer (SP2, DMT) (Schwarz et al., 2010) for the measurement of rBCc concentrations. The minimum mass-equivalent diameter of rBC core that can be detected by SP2 is 70 nm using a rBC material density of 1.8 g/cm^3 . The volume properties of non-refractory material within rBCc (hence referred as 'coating thickness') was derived by SP2 leading-edge-only (LEO) method and is described as the ratio between the optical volume-equivalent diameter of total rBCc and the mass-equivalent diameter of rBC core (D_p/D_c) (Liu et al., 2019). Previous

morphology-independent measurement study validated that the uncertainty of the SP2 LEO fitting method in determining the rBCc coating thickness is within 20% (Yu et al., 2020). A cloud condensation nuclei counter (CCNc, DMT) was used to sample the potential CCN activation ability at a constant supersaturation (SS) of 0.2% and a condensation particle counter (CPC, TSI model 3776) was used to measure the condensation nuclei (CN) number concentration. The SP2 incandescence signal was calibrated using nebulised Aquadag black carbon particle standards while the scattering channel was calibrated by 200 nm polystyrene latex spheres before the measurement, and the standard correction factor of 0.75 for ambient rBC measurement was applied (Laborde et al., 2012). The ionization efficiency of AMS was calibrated using mono-disperse ammonium nitrate particles following the standard protocols (Xu et al., 2017), and a constant collection efficiency (CE) of 0.5 was applied (Middlebrook et al., 2012). More details of the calibration and operation of this AMS instrument can be seen in previous publications based on field measurement studies (Hu et al., 2021a; Liu et al., 2021). The term 'all particles' in this study is referred as the PM_1 compositions including Organic compounds (Org), Sulfate (SO_4), ammonia (NH_4), Nitrate (NO_3), Chloride (Cl) and rBC from AMS and SP2. The AAC was set to classify dry aerosol particles from 90 nm to 1100 nm in aerodynamic diameter (D_a) to cover the detection range of the SP2 and AMS. It took around 15 min to complete one scan using the AAC step scanning mode, and a timed valve was placed at the upstream of the AAC for switching between monodisperse and polydisperse every 30 min. Example for a running cycle is presented in the supplementary.

2.2 Calculation of size-resolved aerosol morphology parameters

The dynamic shape factor (χ) describes the shape of particles (Decarlo et al., 2004). χ = 1 denotes a perfectly spherical particle, and χ > 1 means more non-sphericity. Based on the size-resolved measurement here, χ can be calculated by:

$$\chi = \frac{\rho_p {D_v}^2 C_c(D_v)}{{D_a}^2 C_c(D_a)} \quad (1)$$

where ρ_p is the particle material density, C_c represents the slip correction factor at a given diameter and is calculated following the description in Kim et al. (2005), D_v is the particle volume equivalent diameter, and D_a is the aerodynamic diameter classified by AAC. This calculation is performed for all particles (including rBCc)

and rBCc at each size bin, using their respective parameters (ρ_p and D_v). For all particles, ρ_p is the mean density weighted by the PM_1 results measured by the AMS and SP2. Mineral dust particles are not measured during the experiment because of the instrument upper detection limit. Mineral dust particles are mainly externally mixed with other aerosol compositions and mostly in coarse mode (with $D_a > 1$ μm) (Seinfeld and Pandis, 2016), and there was no dust event during the experimental periods. Previous measurements showed that mineral dust particle only accounted ~10% of total PM_1 mass concentration in Beijing (Zhang et al., 2018), and most of them were at $D_a > 500$ nm (Li et al., 2014). Therefore, our results may slightly underestimate the ρ_{all} and total particle mass (M_{all}) in bins with $D_a > 500$ nm if dust is present, although we consider this effect to be minor. To compute the particle volume results based on the AMS measured ion and Org concentrations, a simplified ion pairing scheme presented in Gysel et al. (2007) was applied, and the solutions are described in the supplementary. The ρ_p of rBCc is calculated as the weighted density within rBCc including rBC and coatings, where the coating material of rBCc is assumed to constitute of the same volume fractions of ambient non-refractory compositions (Liu et al., 2015; Hu et al., 2021a):

$$\rho_{rBCc} = \frac{M_{rBCc}}{V_{rBCc}} = \frac{\rho_{NR} \cdot \left(\frac{1}{6}\pi D_{p,rBCc}^3 - \frac{1}{6}\pi D_c^3\right) + M_{rBC}}{\frac{1}{6}\pi D_{p,rBCc}^3} \quad (2)$$

where M_{rBCc} and V_{rBCc} are the mass and volume of the rBCc respectively, ρ_{NR} is the particle density of non-refractory compositions. The rBC core diameter (D_c) and total rBCc diameter ($D_{p,rBCc}$) are derived through the SP2 LEO method.

For all particles, mean single particle mass is derived from the total mass (M_{all}) obtained by AMS and SP2 divided by the total number (N_{total}) obtained by the CPC, hereinafter the mean D_v of particle is assumed to equal to the mass equivalent diameter (D_m) and is obtained by applying the mean ρ_p above:

$$D_{v,all} = D_{m,all} = \sqrt[3]{\frac{6M_{single,all}}{\rho_{all} \cdot \pi}} = \sqrt[3]{\frac{6M_{all}}{\rho_{all} \cdot \pi \cdot N_{total}}} \quad (3)$$

where ρ_{all} is the particle density of all aerosol particles. The parameters used for the calculation is also listed in Appendix A.

2.3 Hygroscopicity parameter calculation

The hygroscopicity parameter (κ) (Petters and Kreidenweis, 2007) of measured aerosols is predicted based on the measured aerosol compositions and invoking the Zdanovskii–Stokes–Robinson (ZSR) mixing rule(Stokes and Robinson, 1966). The κ for all particles (κ_{all}) is calculated as:

$$\kappa_{all} = \sum_i \varepsilon_i \kappa_i \quad (4)$$

where ε_i and κ_i is the volume fraction and hygroscopicity parameter of each chemical composition respectively. The κ based on the AMS measured concentrations were calculated based on the same simplified ion pairing scheme described above. The detailed information for each parameter used for κ calculation is listed in Table S1. For rBCc, the κ_{rBCc} is calculated by:

$$\kappa_{rBCc} = \sum_i \varepsilon_{coating,i} \kappa_{coating,i} + \varepsilon_{rBC} \kappa_{rBC} \quad (5)$$

Where $\varepsilon_{\mathrm{coating},i}$ and $\varepsilon_{\mathrm{rBC}}$ is the volume fraction coating and rBC respectively; $\kappa_{\mathrm{coating},i}$ represents the hygroscopicity parameter for each rBCc coating composition and is assumed to equal to the κ of ambient non-refractory compositions (Motos et al., 2019b; Hu et al., 2021a); κ_{rBC} represents the hygroscopicity parameter for rBC and the last term can be ignored since pure rBC is assumed to be hydrophobic. Due to the coating material of rBCc is not included in the calculation process of κ_{all} here, κ_{all} may be slightly underestimated when rBCc is thickly coated at larger particle size.

2.4 CCN ability of all particles and rBCc

The CCN activation fraction is determined as the ratio between CCN number concentration at SS=0.2% and the CN number concentration measured by the CPC. The size-resolved CCN activation fraction (*AF*) is fitted with a sigmoid function:

$$AF = \frac{E}{1+\left(\frac{D_{50}}{D_p}\right)^C} \times 100\% \quad (6)$$

Where E and C are fitting coefficients which represent the asymptote and the slope respectively. D_{p} is the particle dry diameter, and D_{50} represents the critical particle diameter where 50% of particles in number can be activated as CCN (Petters and Kreidenweis, 2007).

The number concentration of rBCc which acts as CCN is derived from the concurrent measurements of rBC number concentration, CCN and CN. The method described by Hu et al. (2021a) has been applied to determine the activation of rBCc. Firstly, the un-activated particle number concentration is derived from the difference between CN and CCN, as the red line in Fig. 2(a) shows. For particles with D_a > 300nm in the example, the un-activated particles are nil thus all rBCc is also activated. Here particles are considered to be well mixed, and rBCc is less hydrophilic than any other non-refractory particles at the same particle size. Thus, the rBCc is more difficult to be activated as CCN than the other particles. For particles with D_a < 300nm, the rBCc is therefore considered to be the first in contributing the un-activated particles and the activated rBCc is the rBCc number concentration higher than the un-activated particle numbers. By this way, the size-dependent activated rBCc number concentration can be obtained (black line in Fig. 2(b)). $D_{50,\,rBCc}$ can then be derived through Equation (6) based on the rBCc activation fraction curve. The rBCc activation fraction derived through this method is further referred as "measured AF_{rBCc}". There may be some occasions when rBCc could exhibit a higher hygroscopicity, if coated with sufficient hygroscopic substances, even higher than a particle without containing rBC. This means the scenario here may underestimate some fractions of activated rBCc. The method here may therefore serve as a minimum estimation of droplet activation of rBCc from this aspect.

The rBCc activation is also estimated through the calculated size-resolved critical supersaturation (SS_c) (Wu et al., 2019; Hu et al., 2021a) for comparison, which is derived based on the κ_{rBCc} described before from the κ-Köhler theory:

$$S(D) = \frac{D^3 - D_{rBCc}^3}{D^3 - D_{rBCc}^3(1-\kappa)} exp\left(\frac{4\sigma_{s/a}M_w}{RT\rho_w D}\right) \quad (7)$$

Where D is the diameter of the droplet, D_{rBCc} is the rBCc dry diameter, M_w and ρ_w are the molecular weight and density of water respectively, T is temperature, R is the ideal gas constant, and $\sigma_{s/a}$ is the surface tension of the solution/air interface. A decreased SS with increasing D_a can be obtained (Fig. 3), so the $D_{50,\,rBCc}$ at SS_c = 0.2% is the cross point above which diameter only SS<0.2% is required to activate the targeting rBCc. The activated rBCc number concentration is the rBCc concentration with size larger than $D_{50,\,rBCc}$. The activation fraction estimated through this method is further referred as "modelled AF_{rBCc}".

2.5 NAME dispersion model

The airmass classification results used to identify potential source regions are generated by the UK Met Office Numerical Atmospheric dispersion Modelling Environment (NAME) dispersion model (Jones et al., 2007). The model presented the 48h backward dispersion results on a $0.25^{\circ} \times 0.25^{\circ}$ grid using the three-dimensional gridded meteorological field generated from the UK Met Office's Unified Model (Brown et al., 2012). Beijing and its surrounding areas have been classified into five regions as shown in Fig. 4(a) in order to attribute the airmass histories: The Local Beijing (39-41.5°N, 115-117°E), the North (41.5-45°N, 104-121°E), the South (32-39°N, 115-121°E), the West (32-41.5°N, 104-115°E) and the East region (39-41.5°N, 117-121°E).

3. Results and discussions

3.1 Overview for the whole campaign period

Fig. 4(c) presents the overview of aerosol total number and mass concentrations during the experimental period. Beijing and its suburban region experience large contrasts in pollution conditions depending on the wind direction (Liu et al., 2019; Chen et al., 2020b). To test whether the aerosol physiochemical properties vary according to ambient pollution concentrations, the pollution is classified into three levels according to the frequency distribution of PM_1 concentrations during the whole measurement period: heavy pollution ($PM_1 \geq 30\ \mu g/m^3$), moderate pollution ($10\ \mu g/m^3 < PM_1 < 30\ \mu g/m^3$), and light pollution ($PM_1 \leq 10\ \mu g/m^3$). Combining the airmass history results with the aerosol optical depth (AOD) spatial distribution results from the Himawari-8 Level 2 aerosol product (Bessho et al., 2016; Fukuda et al., 2013) (Fig. 4(b)), the heavy and moderate pollution period was mostly attributed to airmasses from the East and West regions. While the contribution from the Local airmass cannot be ignored in some pollution cases, relatively clean northerly airmasses were associated with the light pollution periods.

3.2 Size-resolved aerosol mass compositions and rBCc mixing state

Fig. 5(a-e) presents the size-resolved average mass concentrations for PM_1, rBC, organic compounds (Org), sulfate (SO_4), nitrate (NO_3) respectively under each pollution condition. Though the heavy pollution period has the highest aerosol mass

concentrations among three cases, the mass concentrations for total PM_1 and non-refractory compositions were close at D_a < 200 nm under different pollution levels (Fig. 5(a)). Notable contributions to the total PM_1 from non-refractory material was observed for D_a > 300 nm especially for the heavy pollution condition in Fig. 5 (i-k). Unlike the more polluted conditions, the non-refractory aerosol mass concentrations during light pollution periods shows size-dependent variation in a much lower absolute value range. Fig. 5(b) shows that the size distribution of rBC mass concentration reached the peak at 400 nm under heavy pollution, while the peak for the moderate and light pollution was at a smaller D_a which was between 300 and 400 nm. Fig. 5(c-e) show that the peak diameter of NR-PM_1 observed in Pinggu was at around 700 nm and is higher than the peak diameter of NR-PM_1 reported at the urban site of Beijing which is between 400 nm and 500 nm in winter (Hu et al., 2016). Due to the higher primary organic aerosol (POA) emissions, the results at Beijing urban site has higher contribution of Org at smaller size (< 500 nm) (Zhang et al., 2014). The Org peak diameter in Pinggu is at around 700 nm which is close to the peak diameter of secondary inorganic compositions. The average oxygen to carbon ratio (O/C ratio) for the total Org aerosol in Pinggu is 0.5 and is higher than the O/C ratio in Beijing urban region in winter which is 0.32 reported by Hu et al. (2016). These suggest the higher oxidization of Org in Beijing suburban than the urban region. The higher peak diameter of secondary inorganic compound also indicates well mixed aerosol components in suburban region (Liu et al., 2016). This size-resolved composition result reported in Pinggu is consistent with the previous measurement in another suburban region in NCP (Li et al., 2021). Comparing the composition mass fractions under three different pollution cases shown in Fig.5(i-k), one of the remarkable differences is that particulate nitrate accounted a larger mass fraction during the heavy and moderate pollution periods than during the light pollution period. Previous studies shown that this rapid particulate nitrate formation in Beijing area is mainly associated with the heterogeneous hydrolysis of N_2O_5 at night (Li et al., 2018). Particulate nitrate has become one of the major secondary inorganic aerosol pollutants in urban environment recently (Zhang et al., 2015), and NO_3 also contributed to the aerosol hygroscopicity significantly during the haze pollution periods (Sun et al., 2018). Due to the significant reduction of SO_x emissions in China in recent years (Zhang et al., 2012), the mass fractions of SO_4 remained low in pollution cases. The Org contributed to the aerosol mass compositions significantly, and the capping of rBC mass fraction was around 25% among all three cases.

Fig. 5(f) and (g) present the size distribution of rBC core mass median diameter (MMD) and the coating thickness. This indicates larger D_a had selected rBCc with larger rBC core and higher coatings. The MMD of rBC core increased from below 100 nm to around 300 nm with the increasing of particle size. The rBC core for the light pollution condition was a little smaller than the other two periods, indicating a possible coagulation process in more polluted cases with higher rBC concentrations. The coating thickness of rBCc D_p/D_c decreased slightly when D_a increased from 90 to 300 nm This decreasing trend of rBC coating thickness may be caused by the local traffic emissions. Studies have shown that fresh traffic diesel engine emitted rBCc importantly contribute to the condensation mode particles with diameters of 100-300 nm (Seinfeld and Pandis, 2016; Gong et al., 2016). Joshi et al. (2021) demonstrated that traffic emissions dominated the rBC fluxes in Beijing, and previous studies also showed a similar decreasing trend of rBC coatings for engine emissions within this particle size range (Han et al., 2019; Zhang et al., 2020). According to the diffusion-controlled particle growth law, smaller particles diffuse more quickly and hence grow more effectively than the larger particles (Seinfeld and Pandis, 2016). Therefore, smaller rBC acquire more coatings within particle diameters of 100-300 nm. Limited differences were observed for the size-resolved D_p/D_c among the three pollution levels. The average D_p/D_c for all rBCc was 2.1 ± 0.2, 1.6 ± 0.1, and 1.5 ± 0.04 for heavy, moderate and light pollution respectively. There was more heavily coated rBCc showed for heavy pollution condition, and this was consistent with more secondary particle formation than the other periods.

Fig. 5(h) shows the distribution of hygroscopicity parameter (κ). The lowest κ_{all} between 150 and 300 nm at heavy and moderate pollution condition was mainly caused by the increasing of rBC fractions. Due to the increase of more hydroscopic inorganic compositions for larger particles under heavy and moderate pollution conditions, κ_{all} increased considerably for particles D_a > 200 nm and 300 nm. In contrast to the more polluted cases, κ_{all} under light pollution period varied slightly with the increase of D_a. Caused by the absence of more soluble inorganic compositions, κ_{all} for particles with D_a > 300 nm during light pollution period was lower than the other conditions. For

rBCc, κ_{rBCc} was more influenced by the coating volume fractions rather than the coating compositions, as the variation of κ_{rBCc} generally followed the trend of rBCc coating thickness (Fig. 5(g)). κ_{rBCc} for particles with D_a < 300 nm was close under three different pollution levels, and the decreasing trend of κ_{rBCc} between 90 and 300 nm was caused by the reduction of coating material fraction.

3.3 Size-resolved particle morphology

Fig. 6 shows the distribution of particle density, average single particle size and mass, and morphology parameters for all particles (left) and rBCc (right). The average particle density for all particles (ρ_{all}) varied slightly between 1.55 and 1.6 $\mathrm{g/cm^3}$, and the rBCc particle density (ρ_{rBCc}) within the measurement size range was generally higher than the ρ_{all} due to the higher density of rBC. The peak ρ_{rBCc} reached at between 200 and 300 nm in D_a due to the rBCc was least coated within this size range. D_v was larger than D_a and deviated more at smaller size but was close to D_a for all particles and rBCc larger than 200 nm. The dynamic shape factor (χ) of all particles declined from around 1.8 to 1.2, while χ of rBCc declined from around 2 to 1.2. All particles with D_a above 400 nm and rBCc with D_a above 500 nm tended to have lower χ which was around 1.2. Previous study (Lin et al., 2015) in other megacities reported that χ of all particles was around 2 with D_a at around 100 nm which is close to our results.

This result indicates that smaller particles have more irregular shapes, while particles with larger aerodynamic size are more spherical in ambient atmosphere. Previous experiments have shown that the irregular rBCc from fresh emissions can transform to be more spherical-like by acquiring more secondary substances (Ahern et al., 2016). Hu et al. (2021b) illustrates that the acquisition of coating material is more important for the overall rBCc shape, while the shape of rBC core is not sufficient to describe the change of overall rBCc shape. Our results confirm that the spherical assumption is suitable for large rBCc in aerodynamic size in a typical anthropogenic polluted environment. This also implies that larger and spherical particles tend to have larger deposition rate, while particles with more irregularity may experience higher drag force in the air, towards decelerating the settlement.

3.4 Size-resolved CN and CCN number concentrations

Fig.7(a) and (b) presents the distribution of rBCc, CN and CCN number concentrations at different polluted conditions. The peak of rBCc number concentration during heavy pollution periods was at around 300 nm, while the peak for moderate and light pollution was slightly smaller (at around 200 nm). This agrees with the previous studies in Beijing showing that the average total rBCc particles size was associated with the pollution levels (Yu et al., 2020; Liu et al., 2019). A similar trend was also observed for the CN concentrations, and the peak of CN concentrations shifted to the larger particle size with increasing pollution levels. Higher levels of pollution enlarged the particle size through condensation and coagulation. Because of the increasing of average particle size, a larger fraction of particles can be activated as CCN under heavy pollution.

By using aerodynamic size-resolved number concentration of rBC and CN, a remarkable increase of rBC number fraction at larger aerodynamic size was found (Fig 7(c)), i.e. with D_a from 100-1000nm, rBC number fraction increased almost linearly from 3% to 15%, and this applied to all pollution levels. This tends to represent a generic phenomenon for a suburban environment with continuous influence of anthropogenic emissions, and the primary emissions had been aged in a time scale of hours. Fine rBC coagulated with pre-existing larger particles during the aging process (Riemer et al., 2009). The coagulation process dominated the formation of thickly-coated rBC particles (Reddington et al., 2013), and the coagulation rate of smaller rBC may be fast due to the higher number concentration of fine mode particles (Matsui et al., 2018). The coagulation occurs more rapidly near source due to the higher number concentration (Jacobson, 2005). Zhang et al. (2020) reported an increase in BC number concentrations with increasing rBC core size for fresh residential firewood burning emission in Beijing surrounding regions. Due to the high concentration of both rBC and co-emitted NR particles, the coagulation of rBC is rapid and thickly coated rBCc with relatively large rBC core formed shortly after emission. Liu et al. (2019) also reported higher aging degree of rBCc during the heating season in North China. However, the very fresh fossil fuel emissions such as from diesel engine emissions, which mostly contains thinly-coated small rBC (Han et al., 2019), may not show the same rBC number fraction distribution. Previous studies also reported a relatively fast aging process for BC also in the order of hours (Peng et al., 2017), if under a polluted environment rich of precursors, the aging could be even faster (Peng et al., 2016). The cause of this increased rBC number fraction at larger particle size is therefore the non-

rBC compounds associated with it. The results presented here indicated that the higher contribution from regional pollution to the rBC number at larger aerodynamic size may apply, albeit the various features of primary sources in winter (Wang et al., 2019; Liu et al., 2019).

It is also possible that these larger rBCc may have experienced in-cloud processing. If the air parcel has passed through a cloud, the large and thickly coated rBCc are expected to have be scavenged through activation, and the size of rBC core may increase effectively within the cloud because of the cloud droplet collision (Ding et al., 2019b). Through in-cloud aqueous reactions, sulphate or organic matter may be added to the rBCc (Zhang et al., 2017). When the cloud dries out through the cloud evaporation or the air parcel descending in a downdraft, the core size and coatings may be enlarged for these released rBCc. Although the results presented here cannot alone test this hypothesis.

The rBC associated with larger coatings was more spherical (with χ close to 1, as discussed above), therefore more likely to have an absorption enhancement from the lensing effect of coatings (Liu et al., 2017). In addition, this size-resolved rBC number fraction results will improve the understanding to the lung deposition of BC in human health studies (Rissler et al., 2017). This means for particles with higher deposition rate tend to contain a higher number fraction of rBC, which may provide some indications for constituents deposited on different parts in human respiratory system (Carvalho et al., 2011; Manigrasso et al., 2020).

3.5 CCN ability and rBCc activation

Presented in Fig. 8(a), the $D_{50,\,\mathrm{All}}$ varied smoothly and was slightly higher than 100 nm for most of the experiment period. The mean $D_{50,\,\mathrm{All}}$ and $D_{50,\,\mathrm{rBCc}}$ was 112 ± 6 nm and 193 ± 41 nm respectively. Shown in Fig. 8(d) most of the $D_{50,\,\mathrm{rBCc}}$ was around 200 nm which illustrates that the number concentrations of rBCc with D_a above 200 nm had significant contribution to the overall AF_{rBCc}.

Fig. 8(b) presents the temporal evolution of the CCN number concentration and activation fraction for all particles and rBCc. Fig. 8(e) showed 50 ± 4% of the measured

particles can be activated with SS=0.2% under heavy polluted period, while the AF_{all} for the light pollution period was generally lower than the AF_{all} of the other two periods which was 24 ± 10% on average. The AF_{all} for the moderate pollution period was 39 ± 9% on average. Shown in Fig. 8(e) and (f), both all particles and rBCc showed high activation fraction of around 50% during the heavy pollution periods. While for moderate and light pollution conditions, rBCc exhibited substantially higher activation fraction than all particles, especially under light pollution periods where the average activation fraction was 44 ± 18% for rBCc compared to 24 ± 10% for all particles. The maintaining high rBCc activation fraction at all pollution levels resulted from the relatively higher rBC number fractions at larger D_a (Fig. 8(c)) because of the higher associated coatings. The directly measured CCN activity of rBCc showed that particles at larger sizes had contained a larger fraction of rBCc that were CCN active, due to the larger particle size. This in turn implies that the rBCc has the potential to be more efficiently incorporated into cloud droplets. The measured and modelled AF_{rBCc} was close and agreed within 22% (shown in Fig. S3), and the modelled AF_{rBCc} was slightly higher than the measurement results. This underestimation of modelled $D_{50,\,rBCc}$ may result from an overestimation on the κ_{rBCc} as here a consistent κ was applied between rBCc coatings and all non-refractory materials in bulk, though the coatings on rBC may have not contained as much hygroscopic materials as the bulk non-rBC aerosols. Freshly emitted rBC particles contain substantial amounts of organic matter (Peng et al., 2017) while the more hygroscopic secondary inorganic materials require atmospheric aging to be mixed with rBC (Hu et al., 2020b). Our results confirm that while rBCc can be CCN active, the size of rBCc is crucial to the rBCc CCN ability in polluted suburban environment. This agrees with the previous study done by Motos et al. (2019b) who also found that the size of rBCc is important for rBCc activation at certain SS. The AF_{rBCc} result presented in our study is generally consistent with previous field measurements in anthropogenic polluted environments in China: Wu et al. (2019) and Hu et al. (2021a) reported 59% and 60% of total rBCc could be activated at SS = 0.2% respectively. Studies performed in other environments also found that coated BC can be CCN active: Motos et al. (2019a) and (2019b) reported that ~6%-12% and ~40%-70% of total BC mass fraction can be activated with SS ≈ 0.05% in Zurich and SS ≈ 0.2% at Jungfraujoch respectively.

4. Atmospheric implications

The AAC combination applied in this study introduced a new way to explore the physiochemical properties of aerosols. The comprehensive size-resolved aerosol information presented in this study can contribute to future studies focusing on the BC evolution and lifetime, and improve the particle resolved model simulations (i.e. Riemer et al. (2009)) for the anthropogenic polluted environment. Importantly, our results shown that thickly coated rBCc accounted higher number fraction at larger particle size than the smaller particle size in Beijing suburban. As indicated in Fig. 9, the mass absorption coefficient (MAC) of rBCc at 550 nm and 880 nm wavelength is calculated through the core-shell Mie model described in the supplementary. The MAC_{550} and MAC_{880} was about 2-fold enhanced for rBCc with D_a > 500 nm. These larger rBCc with high absorption efficiency importantly contributed to the total absorption. When transported into the top of boundary layer, these highly coated and absorbing rBCc can be efficiently incorporated into clouds (Ding et al., 2019a). The absorption effects of these rBCc will be further magnified by mixing with the cloud water droplets (Wu et al., 2016), and the lensing effect may reduce the cloud lifetime (Ramanathan et al., 2001) or the cloud albedo (Chuang et al., 2002). In addition to the strong radiative absorption, these large rBCc may also alter the regional precipitation rate (Johnson et al., 2019).

Conclusions

In this study, a new aerodynamic size selection technique was applied for the direct size-resolved characterisation of aerosol constituents and properties on both mass and number basis in a suburban Beijing in winter. Besides the size selection without relying on particle charging efficiency, this technique allows reliable size-resolved particle properties. Organic compound accounted around 40% of the total PM_1 mass, and we found higher contribution of particulate nitrate at larger sizes under polluted cases in Beijing suburban. In particular, particles with larger aerodynamic diameter (D_a) were found to contain a higher number fraction of refractory black carbon (rBC), which means rBC could be more efficiently mixed with larger particles during atmospheric processes. Mie calculation results show that these thickly coated rBC containing particles (rBCc) as included in large particle may have an up to 2-fold of enhanced absorption. The dynamic shape factors for both refractory and non-refractory particles

have also been derived. Particles with D_a larger than 300 nm tended to have a more spherical-like shape, while smaller particles were with more irregular shape in the polluted environment. By applying the method introduced by Hu et al. (2021a), as high as 46 ± 15% number fraction of rBCc was observed to be activated under SS=0.2%. Our results suggest that the size of rBCc is key to the cloud condensation nuclei (CCN) activities of rBCc. Though rBC was small and hydrophobic initially, after being mixed with non-refractory compositions and becoming larger, the rBCc can become CCN active. The higher number fraction of rBCc at larger particle size (D_a > 300 nm) emphasizes the importance of the rBCc as a considerable CCN source. In summary, the rBCc from anthropogenic emissions, after short aging in regional scale, may therefore alter the regional radiative forcing directly or indirectly through altering cloud properties and deposit on human respiratory system efficiently.

Acknowledgments

This research was supported by the National Natural Science Foundation of China (Grant Nos. 42175116，41875167, 41975177), and the National Key Research and Development Program of China (2019YFC0214703). The authors acknowledge the Cambustion Ltd for providing the AAC instrument.

Author Contribution

CY and DL deigned the experiments and wrote the paper; DL and JDA provided guidance with the analysis and writing; CY, DL, KH, PT, YW, DZ, WG, MH and DD performed experiments; CY, DL, KH, HW, DH and JDA contributed to the data analysis; QL provided the AAC and guided the operations.

Data availability

Raw data is archived at Zhejiang University and is available on request.

Competing financial interests

The authors declare no competing financial interests.

References

Ahern, A. T., Subramanian, R., Saliba, G., Lipsky, E. M., Donahue, N. M., and Sullivan, R. C.: Effect of secondary organic aerosol coating thickness on the real-time detection and characterization of biomass-burning soot by two particle mass spectrometers, Atmos. Meas. Tech., 9, 6117-6137, 10.5194/amt-9-6117-2016, 2016.

Bessho, K., Date, K., Hayashi, M., Ikeda, A., Imai, T., Inoue, H., Kumagai, Y., Miyakawa, T., Murata, H., Ohno, T., Okuyama, A., Oyama, R., Sasaki, Y., Shimazu, Y., Shimoji, K., Sumida, Y., Suzuki, M., Taniguchi, H., Tsuchiyama, H., Uesawa, D., Yokota, H., and Yoshida, R.: An Introduction to Himawari-8/9— Japan’s New-Generation Geostationary Meteorological Satellites, Journal of the Meteorological Society of Japan. Ser. II, 94, 151-183, 10.2151/jmsj.2016-009, 2016.

Bond, T. C., Doherty, S. J., Fahey, D. W., Forster, P. M., Berntsen, T., DeAngelo, B. J., Flanner, M. G., Ghan, S., Kärcher, B., Koch, D., Kinne, S., Kondo, Y., Quinn, P. K., Sarofim, M. C., Schultz, M. G., Schulz, M., Venkataraman, C., Zhang, H., Zhang, S., Bellouin, N., Guttikunda, S. K., Hopke, P. K., Jacobson, M. Z., Kaiser, J. W., Klimont, Z., Lohmann, U., Schwarz, J. P., Shindell, D., Storelvmo, T., Warren, S. G., and Zender, C. S.: Bounding the role of black carbon in the climate system: A scientific assessment, Journal of Geophysical Research: Atmospheres, 118, 5380-5552, https://doi.org/10.1002/jgrd.50171, 2013.

Broekhuizen, K., Chang, R. Y. W., Leaitch, W. R., Li, S. M., and Abbatt, J. P. D.: Closure between measured and modeled cloud condensation nuclei (CCN) using size-resolved aerosol compositions in downtown Toronto, Atmos. Chem. Phys., 6, 2513-2524, 10.5194/acp-6-2513-2006, 2006.

Brown, A., Milton, S., Cullen, M., Golding, B., Mitchell, J., and Shelly, A.: Unified Modeling and Prediction of Weather and Climate: A 25-Year Journey, Bulletin of the American Meteorological Society, 93, 1865-1877, 10.1175/BAMS-D-12-00018.1, 2012.

Cappa, C. D., Onasch, T. B., Massoli, P., Worsnop, D. R., Bates, T. S., Cross, E. S., Davidovits, P., Hakala, J., Hayden, K. L., Jobson, B. T., Kolesar, K. R., Lack, D. A., Lerner, B. M., Li, S.-M., Mellon, D., Nuaaman, I., Olfert, J. S., Petäjä, T., Quinn, P. K., Song, C., Subramanian, R., Williams, E. J., and Zaveri, R. A.: Radiative Absorption Enhancements Due to the Mixing State of Atmospheric Black Carbon, Science, 337, 1078, 10.1126/science.1223447, 2012.

Carvalho, T. C., Peters, J. I., and Williams, R. O.: Influence of particle size on regional lung deposition – What evidence is there?, International Journal of Pharmaceutics, 406, 1-10, https://doi.org/10.1016/j.ijpharm.2010.12.040, 2011.

Chen, Y., Cai, J., Wang, Z., Peng, C., Yao, X., Tian, M., Han, Y., Shi, G., Shi, Z., Liu, Y., Yang, X., Zheng, M., Zhu, T., He, K., Zhang, Q., and Yang, F.: Simultaneous measurements of urban and rural particles in Beijing – Part 1: Chemical composition and mixing state, Atmos. Chem. Phys., 20, 9231-9247, 10.5194/acp-20-9231-2020, 2020a.

Chen, Y., Shi, G., Cai, J., Shi, Z., Wang, Z., Yao, X., Tian, M., Peng, C., Han, Y., Zhu, T., Liu, Y., Yang, X., Zheng, M., Yang, F., Zhang, Q., and He, K.: Simultaneous measurements of urban and rural particles in Beijing – Part 2: Case studies of haze events and regional transport, Atmos. Chem. Phys., 20, 9249-9263, 10.5194/acp-20-9249-2020, 2020b.

Ching, J. and Kajino, M.: Aerosol mixing state matters for particles deposition in human respiratory system, Scientific Reports, 8, 8864, 10.1038/s41598-018-27156-z, 2018.

Chuang, C. C., Penner, J. E., Prospero, J. M., Grant, K. E., Rau, G. H., and Kawamoto,

627 K.: Cloud susceptibility and the first aerosol indirect forcing: Sensitivity to black carbon
628 and aerosol concentrations, Journal of Geophysical Research: Atmospheres, 107, AAC
629 10-11-AAC 10-23, https://doi.org/10.1029/2000JD000215, 2002.
630 DeCarlo, P. F., Slowik, J. G., Worsnop, D. R., Davidovits, P., and Jimenez, J. L.:
631 Particle Morphology and Density Characterization by Combined Mobility and
632 Aerodynamic Diameter Measurements. Part 1: Theory, Aerosol Science and
633 Technology, 38, 1185-1205, 10.1080/027868290903907, 2004.
634 DeCarlo, P. F., Kimmel, J. R., Trimborn, A., Northway, M. J., Jayne, J. T., Aiken, A.
635 C., Gonin, M., Fuhrer, K., Horvath, T., Docherty, K. S., Worsnop, D. R., and Jimenez,
636 J. L.: Field-Deployable, High-Resolution, Time-of-Flight Aerosol Mass Spectrometer,
637 Analytical Chemistry, 78, 8281-8289, 10.1021/ac061249n, 2006.
638 Ding, S., Liu, D., Zhao, D., Hu, K., Tian, P., Zhou, W., Huang, M., Yang, Y., Wang,
639 F., Sheng, J., Liu, Q., Kong, S., Cui, P., Huang, Y., He, H., Coe, H., and Ding, D.: Size-
640 Related Physical Properties of Black Carbon in the Lower Atmosphere over Beijing
641 and Europe, Environmental Science & Technology, 53, 11112-11121,
642 10.1021/acs.est.9b03722, 2019a.
643 Ding, S., Zhao, D., He, C., Huang, M., He, H., Tian, P., Liu, Q., Bi, K., Yu, C., Pitt, J.,
644 Chen, Y., Ma, X., Chen, Y., Jia, X., Kong, S., Wu, J., Hu, D., Hu, K., Ding, D., and
645 Liu, D.: Observed Interactions Between Black Carbon and Hydrometeor During Wet
646 Scavenging in Mixed-Phase Clouds, Geophysical Research Letters, 46, 8453-8463,
647 https://doi.org/10.1029/2019GL083171, 2019b.
648 Fan, X., Liu, J., Zhang, F., Chen, L., Collins, D., Xu, W., Jin, X., Ren, J., Wang, Y.,
649 Wu, H., Li, S., Sun, Y., and Li, Z.: Contrasting size-resolved hygroscopicity of fine
650 particles derived by HTDMA and HR-ToF-AMS measurements between summer and
651 winter in Beijing: the impacts of aerosol aging and local emissions, Atmos. Chem. Phys.,
652 20, 915-929, 10.5194/acp-20-915-2020, 2020.
653 Fierce, L., Onasch, T. B., Cappa, C. D., Mazzoleni, C., China, S., Bhandari, J.,
654 Davidovits, P., Fischer, D. A., Helgestad, T., Lambe, A. T., Sedlacek, A. J., Smith, G.
655 D., and Wolff, L.: Radiative absorption enhancements by black carbon controlled by
656 particle-to-particle heterogeneity in composition, Proceedings of the National Academy
657 of Sciences, 117, 5196, 10.1073/pnas.1919723117, 2020.
658 Fukuda, S., Nakajima, T., Takenaka, H., Higurashi, A., Kikuchi, N., Nakajima, T. Y.,
659 and Ishida, H.: New approaches to removing cloud shadows and evaluating the 380 nm
660 surface reflectance for improved aerosol optical thickness retrievals from the
661 GOSAT/TANSO-Cloud and Aerosol Imager, Journal of Geophysical Research:
662 Atmospheres, 118, 13,520-513,531, https://doi.org/10.1002/2013JD020090, 2013.
663 Gong, X., Zhang, C., Chen, H., Nizkorodov, S. A., Chen, J., and Yang, X.: Size
664 distribution and mixing state of black carbon particles during a heavy air pollution
665 episode in Shanghai, Atmos. Chem. Phys., 16, 5399-5411, 10.5194/acp-16-5399-2016,
666 2016.
667 Gunthe, S. S., Rose, D., Su, H., Garland, R. M., Achtert, P., Nowak, A., Wiedensohler,
668 A., Kuwata, M., Takegawa, N., Kondo, Y., Hu, M., Shao, M., Zhu, T., Andreae, M. O.,
669 and Pöschl, U.: Cloud condensation nuclei (CCN) from fresh and aged air pollution in
670 the megacity region of Beijing, Atmos. Chem. Phys., 11, 11023-11039, 10.5194/acp-
671 11-11023-2011, 2011.
672 Gysel, M., Crosier, J., Topping, D. O., Whitehead, J. D., Bower, K. N., Cubison, M. J.,
673 Williams, P. I., Flynn, M. J., McFiggans, G. B., and Coe, H.: Closure study between
674 chemical composition and hygroscopic growth of aerosol particles during TORCH2,
675 Atmos. Chem. Phys., 7, 6131-6144, 10.5194/acp-7-6131-2007, 2007.
676 Han, C., Li, S. M., Liu, P., and Lee, P.: Size Dependence of the Physical Characteristics

of Particles Containing Refractory Black Carbon in Diesel Vehicle Exhaust, Environ Sci Technol, 53, 137-145, 10.1021/acs.est.8b04603, 2019.
Han, Y., Chen, W., Chatzidiakou, L., Krause, A., Yan, L., Zhang, H., Chan, Q., Barratt, B., Jones, R., Liu, J., Wu, Y., Zhao, M., Zhang, J., Kelly, F. J., Zhu, T., and the, A. t.: Effects of AIR pollution on cardiopuLmonary disEaSe in urban and peri-urban reSidents in Beijing: protocol for the AIRLESS study, Atmos. Chem. Phys., 20, 15775-15792, 10.5194/acp-20-15775-2020, 2020.
Hu, D., Wang, Y., Yu, C., Xie, Q., Yue, S., Shang, D., Fang, X., Joshi, R., Liu, D., Allan, J., Wu, Z., Hu, M., Fu, P., and McFiggans, G.: Vertical profile of particle hygroscopicity and CCN effectiveness during winter in Beijing: insight into the hygroscopicity transition threshold of black carbon, Faraday Discuss, 10.1039/d0fd00077a, 2020a.
Hu, D., Liu, D., Kong, S., Zhao, D., Wu, Y., Li, S., Ding, S., Zheng, S., Cheng, Y., Hu, K., Deng, Z., Wu, Y., Tian, P., Liu, Q., Huang, M., and Ding, D.: Direct Quantification of Droplet Activation of Ambient Black Carbon Under Water Supersaturation, Journal of Geophysical Research: Atmospheres, 126, e2021JD034649, https://doi.org/10.1029/2021JD034649, 2021a.
Hu, D., Liu, D., Zhao, D., Yu, C., Liu, Q., Tian, P., Bi, K., Ding, S., Hu, K., Wang, F., Wu, Y., Wu, Y., Kong, S., Zhou, W., He, H., Huang, M., and Ding, D.: Closure Investigation on Cloud Condensation Nuclei Ability of Processed Anthropogenic Aerosols, Journal of Geophysical Research: Atmospheres, 125, 10.1029/2020jd032680, 2020b.
Hu, K., Liu, D., Tian, P., Wu, Y., Deng, Z., Wu, Y., Zhao, D., Li, R., Sheng, J., Huang, M., Ding, D., Li, W., Wang, Y., and Wu, Y.: Measurements of the Diversity of Shape and Mixing State for Ambient Black Carbon Particles, Geophysical Research Letters, 48, e2021GL094522, https://doi.org/10.1029/2021GL094522, 2021b.
Hu, W., Hu, M., Hu, W., Jimenez, J. L., Yuan, B., Chen, W., Wang, M., Wu, Y., Chen, C., Wang, Z., Peng, J., Zeng, L., and Shao, M.: Chemical composition, sources, and aging process of submicron aerosols in Beijing: Contrast between summer and winter, Journal of Geophysical Research: Atmospheres, 121, 1955-1977, https://doi.org/10.1002/2015JD024020, 2016.
Jacobson, M. Z.: Fundamentals of Atmospheric Modeling, 2, Cambridge University Press, Cambridge, DOI: 10.1017/CBO9781139165389, 2005.
Johnson, B. T., Haywood, J. M., and Hawcroft, M. K.: Are Changes in Atmospheric Circulation Important for Black Carbon Aerosol Impacts on Clouds, Precipitation, and Radiation?, Journal of Geophysical Research: Atmospheres, 124, 7930-7950, https://doi.org/10.1029/2019JD030568, 2019.
Johnson, T. J., Irwin, M., Symonds, J. P. R., Olfert, J. S., and Boies, A. M.: Measuring aerosol size distributions with the aerodynamic aerosol classifier, Aerosol Science and Technology, 52, 655-665, 10.1080/02786826.2018.1440063, 2018.
Jones, A., Thomson, D., Hort, M., and Devenish, B.: The U.K. Met Office's Next-Generation Atmospheric Dispersion Model, NAME III, Air Pollution Modeling and Its Application XVII, Boston, MA, 2007//, 580-589,
Joshi, R., Liu, D., Nemitz, E., Langford, B., Mullinger, N., Squires, F., Lee, J., Wu, Y., Pan, X., Fu, P., Kotthaus, S., Grimmond, S., Zhang, Q., Wu, R., Wild, O., Flynn, M., Coe, H., and Allan, J.: Direct measurements of black carbon fluxes in central Beijing using the eddy covariance method, Atmospheric Chemistry and Physics, 21, 147-162, 10.5194/acp-21-147-2021, 2021.
Kim, J. H., Mulholland, G. W., Kukuck, S. R., and Pui, D. Y. H.: Slip Correction Measurements of Certified PSL Nanoparticles Using a Nanometer Differential

727 Mobility Analyzer (Nano-DMA) for Knudsen Number From 0.5 to 83, J Res Natl Inst
728 Stand Technol, 110, 31-54, 10.6028/jres.110.005, 2005.
729 Kwon, H.-S., Ryu, M. H., and Carlsten, C.: Ultrafine particles: unique physicochemical
730 properties relevant to health and disease, Experimental & Molecular Medicine, 52, 318-
731 328, 10.1038/s12276-020-0405-1, 2020.
732 Laborde, M., Schnaiter, M., Linke, C., Saathoff, H., Naumann, K. H., Möhler, O.,
733 Berlenz, S., Wagner, U., Taylor, J. W., Liu, D., Flynn, M., Allan, J. D., Coe, H., Heimerl,
734 K., Dahlkötter, F., Weinzierl, B., Wollny, A. G., Zanatta, M., Cozic, J., Laj, P.,
735 Hitzenberger, R., Schwarz, J. P., and Gysel, M.: Single Particle Soot Photometer
736 intercomparison at the AIDA chamber, Atmos. Meas. Tech., 5, 3077-3097,
737 10.5194/amt-5-3077-2012, 2012.
738 Lack, D. A. and Cappa, C. D.: Impact of brown and clear carbon on light absorption
739 enhancement, single scatter albedo and absorption wavelength dependence of black
740 carbon, Atmos. Chem. Phys., 10, 4207-4220, 10.5194/acp-10-4207-2010, 2010.
741 Levin, E. J. T., Prenni, A. J., Palm, B. B., Day, D. A., Campuzano-Jost, P., Winkler, P.
742 M., Kreidenweis, S. M., DeMott, P. J., Jimenez, J. L., and Smith, J. N.: Size-resolved
743 aerosol composition and its link to hygroscopicity at a forested site in Colorado, Atmos.
744 Chem. Phys., 14, 2657-2667, 10.5194/acp-14-2657-2014, 2014.
745 Li, H., Zhang, Q., Zheng, B., Chen, C., Wu, N., Guo, H., Zhang, Y., Zheng, Y., Li, X.,
746 and He, K.: Nitrate-driven urban haze pollution during summertime over the North
747 China Plain, Atmos. Chem. Phys., 18, 5293-5306, 10.5194/acp-18-5293-2018, 2018.
748 Li, J., Cao, L., Gao, W., He, L., Yan, Y., He, Y., Pan, Y., Ji, D., Liu, Z., and Wang, Y.:
749 Seasonal variations in the highly time-resolved aerosol composition, sources and
750 chemical processes of background submicron particles in the North China Plain,
751 Atmospheric Chemistry and Physics, 21, 4521-4539, 10.5194/acp-21-4521-2021, 2021.
752 Li, L., Li, M., Huang, Z., Gao, W., Nian, H., Fu, Z., Gao, J., Chai, F., and Zhou, Z.:
753 Ambient particle characterization by single particle aerosol mass spectrometry in an
754 urban area of Beijing, Atmospheric Environment, 94, 323-331,
755 https://doi.org/10.1016/j.atmosenv.2014.03.048, 2014.
756 Lin, G.-Y., Lee, G.-R., Lin, S.-F., Hung, Y.-H., Li, S.-W., Wu, G.-J., Ye, H., Huang,
757 W., and Tsai, C.-J.: Ultrafine Particles and PM2.5 at Three Urban Air Monitoring
758 Stations in Northern Taiwan from 2011 to 2013, Aerosol and Air Quality Research, 15,
759 2305-2317, 10.4209/aaqr.2015.04.0271, 2015.
760 Lipworth, B., Manoharan, A., and Anderson, W.: Unlocking the quiet zone: the small
761 airway asthma phenotype, The Lancet Respiratory Medicine, 2, 497-506,
762 https://doi.org/10.1016/S2213-2600(14)70103-1, 2014.
763 Liu, D., He, C., Schwarz, J. P., and Wang, X.: Lifecycle of light-absorbing
764 carbonaceous aerosols in the atmosphere, npj Climate and Atmospheric Science, 3,
765 10.1038/s41612-020-00145-8, 2020.
766 Liu, D., Allan, J., Whitehead, J., Young, D., Flynn, M., Coe, H., McFiggans, G.,
767 Fleming, Z. L., and Bandy, B.: Ambient black carbon particle hygroscopic properties
768 controlled by mixing state and composition, Atmos. Chem. Phys., 13, 2015-2029,
769 10.5194/acp-13-2015-2013, 2013.
770 Liu, D., Quennehen, B., Darbyshire, E., Allan, J. D., Williams, P. I., Taylor, J. W.,
771 Bauguitte, S. J. B., Flynn, M. J., Lowe, D., Gallagher, M. W., Bower, K. N., Choularton,
772 T. W., and Coe, H.: The importance of Asia as a source of black carbon to the European
773 Arctic during springtime 2013, Atmos. Chem. Phys., 15, 11537-11555, 10.5194/acp-
774 15-11537-2015, 2015.
775 Liu, D., Joshi, R., Wang, J., Yu, C., Allan, J. D., Coe, H., Flynn, M. J., Xie, C., Lee, J.,
776 Squires, F., Kotthaus, S., Grimmond, S., Ge, X., Sun, Y., and Fu, P.: Contrasting

physical properties of black carbon in urban Beijing between winter and summer, Atmos. Chem. Phys., 19, 6749-6769, 10.5194/acp-19-6749-2019, 2019.
Liu, D., Whitehead, J., Alfarra, M. R., Reyes-Villegas, E., Spracklen, Dominick V., Reddington, Carly L., Kong, S., Williams, Paul I., Ting, Y.-C., Haslett, S., Taylor, Jonathan W., Flynn, Michael J., Morgan, William T., McFiggans, G., Coe, H., and Allan, James D.: Black-carbon absorption enhancement in the atmosphere determined by particle mixing state, Nature Geoscience, 10, 184-188, 10.1038/ngeo2901, 2017.
Liu, Q., Liu, D., Wu, Y., Bi, K., Gao, W., Tian, P., Zhao, D., Li, S., Yu, C., Wu, Y., Hu, K., Ding, S., Gao, Q., Wang, F., He, H., Huang, M., and Ding, D.: Reduced volatility of aerosols from surface emission to the top of planetary boundary layer, Atmos. Chem. Phys. Discuss., 2021, 1-19, 10.5194/acp-2021-362, 2021.
Liu, Z., Hu, B., Zhang, J., Yu, Y., and Wang, Y.: Characteristics of aerosol size distributions and chemical compositions during wintertime pollution episodes in Beijing, Atmospheric Research, 168, 1-12, https://doi.org/10.1016/j.atmosres.2015.08.013, 2016.
Manigrasso, M., Costabile, F., Liberto, L. D., Gobbi, G. P., Gualtieri, M., Zanini, G., and Avino, P.: Size resolved aerosol respiratory doses in a Mediterranean urban area: From PM10 to ultrafine particles, Environment International, 141, 105714, https://doi.org/10.1016/j.envint.2020.105714, 2020.
Marple, V. A., Rubow, K. L., and Behm, S. M.: A Microorifice Uniform Deposit Impactor (MOUDI): Description, Calibration, and Use, Aerosol Science and Technology, 14, 434-446, 10.1080/02786829108959504, 1991.
Matsui, H., Hamilton, D. S., and Mahowald, N. M.: Black carbon radiative effects highly sensitive to emitted particle size when resolving mixing-state diversity, Nature Communications, 9, 3446, 10.1038/s41467-018-05635-1, 2018.
Middlebrook, A. M., Bahreini, R., Jimenez, J. L., and Canagaratna, M. R.: Evaluation of Composition-Dependent Collection Efficiencies for the Aerodyne Aerosol Mass Spectrometer using Field Data, Aerosol Science and Technology, 46, 258-271, 10.1080/02786826.2011.620041, 2012.
Motos, G., Schmale, J., Corbin, J. C., Zanatta, M., Baltensperger, U., and Gysel-Beer, M.: Droplet activation behaviour of atmospheric black carbon particles in fog as a function of their size and mixing state, Atmos. Chem. Phys., 19, 2183-2207, 10.5194/acp-19-2183-2019, 2019a.
Motos, G., Schmale, J., Corbin, J. C., Modini, R. L., Karlen, N., Bertò, M., Baltensperger, U., and Gysel-Beer, M.: Cloud droplet activation properties and scavenged fraction of black carbon in liquid-phase clouds at the high-alpine research station Jungfraujoch (3580 m a.s.l.), Atmos. Chem. Phys., 19, 3833-3855, 10.5194/acp-19-3833-2019, 2019b.
Myhre, G. and Samset, B. H.: Standard climate models radiation codes underestimate black carbon radiative forcing, Atmos. Chem. Phys., 15, 2883-2888, 10.5194/acp-15-2883-2015, 2015.
Peng, J., Hu, M., Guo, S., Du, Z., Shang, D., Zheng, J., Zheng, J., Zeng, L., Shao, M., Wu, Y., Collins, D., and Zhang, R.: Ageing and hygroscopicity variation of black carbon particles in Beijing measured by a quasi-atmospheric aerosol evolution study (QUALITY) chamber, Atmos. Chem. Phys., 17, 10333-10348, 10.5194/acp-17-10333-2017, 2017.
Peng, J., Hu, M., Guo, S., Du, Z., Zheng, J., Shang, D., Levy Zamora, M., Zeng, L., Shao, M., Wu, Y.-S., Zheng, J., Wang, Y., Glen, C. R., Collins, D. R., Molina, M. J., and Zhang, R.: Markedly enhanced absorption and direct radiative forcing of black carbon under polluted urban environments, Proceedings of the National Academy of

827 Sciences, 113, 4266, 10.1073/pnas.1602310113, 2016.
828 Petters, M. D. and Kreidenweis, S. M.: A single parameter representation of
829 hygroscopic growth and cloud condensation nucleus activity, Atmos. Chem. Phys., 7,
830 1961-1971, 10.5194/acp-7-1961-2007, 2007.
831 Ramanathan, V., Crutzen, P. J., Kiehl, J. T., and Rosenfeld, D.: Aerosols, Climate, and
832 the Hydrological Cycle, Science, 294, 2119, 10.1126/science.1064034, 2001.
833 Ravishankara, A. R., Rudich, Y., and Wuebbles, D. J.: Physical Chemistry of Climate
834 Metrics, Chemical Reviews, 115, 3682-3703, 10.1021/acs.chemrev.5b00010, 2015.
835 Reddington, C. L., McMeeking, G., Mann, G. W., Coe, H., Frontoso, M. G., Liu, D.,
836 Flynn, M., Spracklen, D. V., and Carslaw, K. S.: The mass and number size
837 distributions of black carbon aerosol over Europe, Atmos. Chem. Phys., 13, 4917-4939,
838 10.5194/acp-13-4917-2013, 2013.
839 Riemer, N., West, M., Zaveri, R. A., and Easter, R. C.: Simulating the evolution of soot
840 mixing state with a particle-resolved aerosol model, Journal of Geophysical Research,
841 114, 10.1029/2008jd011073, 2009.
842 Riemer, N., Ault, A. P., West, M., Craig, R. L., and Curtis, J. H.: Aerosol Mixing State:
843 Measurements, Modeling, and Impacts, Reviews of Geophysics, 57, 187-249,
844 10.1029/2018rg000615, 2019.
845 Rissler, J., Gudmundsson, A., Nicklasson, H., Swietlicki, E., Wollmer, P., and Löndahl,
846 J.: Deposition efficiency of inhaled particles (15-5000 nm) related to breathing pattern
847 and lung function: an experimental study in healthy children and adults, Part Fibre
848 Toxicol, 14, 10-10, 10.1186/s12989-017-0190-8, 2017.
849 Schwarz, J. P., Spackman, J. R., Gao, R. S., Perring, A. E., Cross, E., Onasch, T. B.,
850 Ahern, A., Wrobel, W., Davidovits, P., Olfert, J., Dubey, M. K., Mazzoleni, C., and
851 Fahey, D. W.: The Detection Efficiency of the Single Particle Soot Photometer, Aerosol
852 Science and Technology, 44, 612-628, 10.1080/02786826.2010.481298, 2010.
853 Seinfeld, J. H. and Pandis, S. N.: Atmospheric Chemistry and Physics: From Air
854 Pollution to Climate Change, 3rd Edition, Wiley-Interscience publication, Wiley2016.
855 Shi, Z., Vu, T., Kotthaus, S., Harrison, R. M., Grimmond, S., Yue, S., Zhu, T., Lee, J.,
856 Han, Y., Demuzere, M., Dunmore, R. E., Ren, L., Liu, D., Wang, Y., Wild, O., Allan,
857 J., Acton, W. J., Barlow, J., Barratt, B., Beddows, D., Bloss, W. J., Calzolai, G.,
858 Carruthers, D., Carslaw, D. C., Chan, Q., Chatzidiakou, L., Chen, Y., Crilley, L., Coe,
859 H., Dai, T., Doherty, R., Duan, F., Fu, P., Ge, B., Ge, M., Guan, D., Hamilton, J. F., He,
860 K., Heal, M., Heard, D., Hewitt, C. N., Hollaway, M., Hu, M., Ji, D., Jiang, X., Jones,
861 R., Kalberer, M., Kelly, F. J., Kramer, L., Langford, B., Lin, C., Lewis, A. C., Li, J., Li,
862 W., Liu, H., Liu, J., Loh, M., Lu, K., Lucarelli, F., Mann, G., McFiggans, G., Miller,
863 M. R., Mills, G., Monk, P., Nemitz, E., O'Connor, F., Ouyang, B., Palmer, P. I., Percival,
864 C., Popoola, O., Reeves, C., Rickard, A. R., Shao, L., Shi, G., Spracklen, D., Stevenson,
865 D., Sun, Y., Sun, Z., Tao, S., Tong, S., Wang, Q., Wang, W., Wang, X., Wang, X.,
866 Wang, Z., Wei, L., Whalley, L., Wu, X., Wu, Z., Xie, P., Yang, F., Zhang, Q., Zhang,
867 Y., Zhang, Y., and Zheng, M.: Introduction to the special issue “In-depth study of air
868 pollution sources and processes within Beijing and its surrounding region (APHH-
869 Beijing)”, Atmos. Chem. Phys., 19, 7519-7546, 10.5194/acp-19-7519-2019, 2019.
870 Squires, F. A., Nemitz, E., Langford, B., Wild, O., Drysdale, W. S., Acton, W. J. F., Fu,
871 P., Grimmond, C. S. B., Hamilton, J. F., Hewitt, C. N., Hollaway, M., Kotthaus, S., Lee,
872 J., Metzger, S., Pingintha-Durden, N., Shaw, M., Vaughan, A. R., Wang, X., Wu, R.,
873 Zhang, Q., and Zhang, Y.: Measurements of traffic-dominated pollutant emissions in a
874 Chinese megacity, Atmos. Chem. Phys., 20, 8737-8761, 10.5194/acp-20-8737-2020,
875 2020.
876 Stokes, R. H. and Robinson, R. A.: Interactions in Aqueous Nonelectrolyte Solutions.

I. Solute-Solvent Equilibria, The Journal of Physical Chemistry, 70, 2126-2131, 10.1021/j100879a010, 1966.
Sturm, R.: Theoretical models for dynamic shape factors and lung deposition of small particle aggregates originating from combustion processes, Zeitschrift für Medizinische Physik, 20, 226-234, https://doi.org/10.1016/j.zemedi.2010.04.001, 2010.
Sun, J., Liu, L., Xu, L., Wang, Y., Wu, Z., Hu, M., Shi, Z., Li, Y., Zhang, X., Chen, J., and Li, W.: Key Role of Nitrate in Phase Transitions of Urban Particles: Implications of Important Reactive Surfaces for Secondary Aerosol Formation, Journal of Geophysical Research: Atmospheres, 123, 1234-1243, 10.1002/2017jd027264, 2018.
Tavakoli, F. and Olfert, J. S.: An Instrument for the Classification of Aerosols by Particle Relaxation Time: Theoretical Models of the Aerodynamic Aerosol Classifier, Aerosol Science and Technology, 47, 916-926, 10.1080/02786826.2013.802761, 2013.
Tavakoli, F. and Olfert, J. S.: Determination of particle mass, effective density, mass–mobility exponent, and dynamic shape factor using an aerodynamic aerosol classifier and a differential mobility analyzer in tandem, Journal of Aerosol Science, 75, 35-42, https://doi.org/10.1016/j.jaerosci.2014.04.010, 2014.
Taylor, J. W., Allan, J. D., Allen, G., Coe, H., Williams, P. I., Flynn, M. J., Le Breton, M., Muller, J. B. A., Percival, C. J., Oram, D., Forster, G., Lee, J. D., Rickard, A. R., Parrington, M., and Palmer, P. I.: Size-dependent wet removal of black carbon in Canadian biomass burning plumes, Atmos. Chem. Phys., 14, 13755-13771, 10.5194/acp-14-13755-2014, 2014.
Vu, T. V., Zauli-Sajani, S., Poluzzi, V., and Harrison, R. M.: Factors controlling the lung dose of road traffic-generated sub-micrometre aerosols from outdoor to indoor environments, Air Quality, Atmosphere & Health, 11, 615-625, 10.1007/s11869-018-0568-2, 2018.
Wang, J., Liu, D., Ge, X., Wu, Y., Shen, F., Chen, M., Zhao, J., Xie, C., Wang, Q., Xu, W., Zhang, J., Hu, J., Allan, J., Joshi, R., Fu, P., Coe, H., and Sun, Y.: Characterization of black carbon-containing fine particles in Beijing during wintertime, Atmos. Chem. Phys., 19, 447-458, 10.5194/acp-19-447-2019, 2019.
Wang, J., Ye, J., Liu, D., Wu, Y., Zhao, J., Xu, W., Xie, C., Shen, F., Zhang, J., Ohno, P. E., Qin, Y., Zhao, X., Martin, S. T., Lee, A. K. Y., Fu, P., Jacob, D. J., Zhang, Q., Sun, Y., Chen, M., and Ge, X.: Characterization of submicron organic particles in Beijing during summertime: comparison between SP-AMS and HR-AMS, Atmos. Chem. Phys., 20, 14091-14102, 10.5194/acp-20-14091-2020, 2020.
Wang, L., Zhang, F., Pilot, E., Yu, J., Nie, C., Holdaway, J., Yang, L., Li, Y., Wang, W., Vardoulakis, S., and Krafft, T.: Taking Action on Air Pollution Control in the Beijing-Tianjin-Hebei (BTH) Region: Progress, Challenges and Opportunities, Int J Environ Res Public Health, 15, 10.3390/ijerph15020306, 2018.
West, J. J., Cohen, A., Dentener, F., Brunekreef, B., Zhu, T., Armstrong, B., Bell, M. L., Brauer, M., Carmichael, G., Costa, D. L., Dockery, D. W., Kleeman, M., Krzyzanowski, M., Künzli, N., Liousse, C., Lung, S.-C. C., Martin, R. V., Pöschl, U., Pope, C. A., Roberts, J. M., Russell, A. G., and Wiedinmyer, C.: "What We Breathe Impacts Our Health: Improving Understanding of the Link between Air Pollution and Health", Environmental Science & Technology, 50, 4895-4904, 10.1021/acs.est.5b03827, 2016.
Wu, Q. Z., Wang, Z. F., Gbaguidi, A., Gao, C., Li, L. N., and Wang, W.: A numerical study of contributions to air pollution in Beijing during CAREBeijing-2006, Atmos. Chem. Phys., 11, 5997-6011, 10.5194/acp-11-5997-2011, 2011.
Wu, Y., Liu, D., Wang, J., Shen, F., Chen, Y., Cui, S., Ge, S., Wu, Y., Chen, M., and Ge, X.: Characterization of Size-Resolved Hygroscopicity of Black Carbon-Containing

Particle in Urban Environment, Environ Sci Technol, 53, 14212-14221, 10.1021/acs.est.9b05546, 2019.
Wu, Y., Zhang, R., Tian, P., Tao, J., Hsu, S. C., Yan, P., Wang, Q., Cao, J., Zhang, X., and Xia, X.: Effect of ambient humidity on the light absorption amplification of black carbon in Beijing during January 2013, Atmospheric Environment, 124, 217-223, https://doi.org/10.1016/j.atmosenv.2015.04.041, 2016.
Wu, Z., Zheng, J., Wang, Y., Shang, D., Du, Z., Zhang, Y., and Hu, M.: Chemical and physical properties of biomass burning aerosols and their CCN activity: A case study in Beijing, China, Science of The Total Environment, 579, 1260-1268, https://doi.org/10.1016/j.scitotenv.2016.11.112, 2017.
Xu, W., Sun, Y., Wang, Q., Du, W., Zhao, J., Ge, X., Han, T., Zhang, Y., Zhou, W., Li, J., Fu, P., Wang, Z., and Worsnop, D. R.: Seasonal Characterization of Organic Nitrogen in Atmospheric Aerosols Using High Resolution Aerosol Mass Spectrometry in Beijing, China, ACS Earth and Space Chemistry, 1, 673-682, 10.1021/acsearthspacechem.7b00106, 2017.
Yu, C., Liu, D., Broda, K., Joshi, R., Olfert, J., Sun, Y., Fu, P., Coe, H., and Allan, J. D.: Characterising mass-resolved mixing state of black carbon in Beijing using a morphology-independent measurement method, Atmos. Chem. Phys., 20, 3645-3661, 10.5194/acp-20-3645-2020, 2020.
Zhang, G., Lin, Q., Peng, L., Bi, X., Chen, D., Li, M., Li, L., Brechtel, F. J., Chen, J., Yan, W., Wang, X., Peng, P., Sheng, G., and Zhou, Z.: The single-particle mixing state and cloud scavenging of black carbon: a case study at a high-altitude mountain site in southern China, Atmos. Chem. Phys., 17, 14975-14985, 10.5194/acp-17-14975-2017, 2017.
Zhang, J. K., Sun, Y., Liu, Z. R., Ji, D. S., Hu, B., Liu, Q., and Wang, Y. S.: Characterization of submicron aerosols during a month of serious pollution in Beijing, 2013, Atmos. Chem. Phys., 14, 2887-2903, 10.5194/acp-14-2887-2014, 2014.
Zhang, Q., He, K., and Huo, H.: Cleaning China's air, Nature, 484, 161-162, 10.1038/484161a, 2012.
Zhang, X. Y., Wang, J. Z., Wang, Y. Q., Liu, H. L., Sun, J. Y., and Zhang, Y. M.: Changes in chemical components of aerosol particles in different haze regions in China from 2006 to 2013 and contribution of meteorological factors, Atmos. Chem. Phys., 15, 12935-12952, 10.5194/acp-15-12935-2015, 2015.
Zhang, Y., Zhang, Q., Yao, Z., and Li, H.: Particle Size and Mixing State of Freshly Emitted Black Carbon from Different Combustion Sources in China, Environmental Science & Technology, 54, 7766-7774, 10.1021/acs.est.9b07373, 2020.
Zhang, Y., Lang, J., Cheng, S., Li, S., Zhou, Y., Chen, D., Zhang, H., and Wang, H.: Chemical composition and sources of PM1 and PM2.5 in Beijing in autumn, Science of The Total Environment, 630, 72-82, https://doi.org/10.1016/j.scitotenv.2018.02.151, 2018.

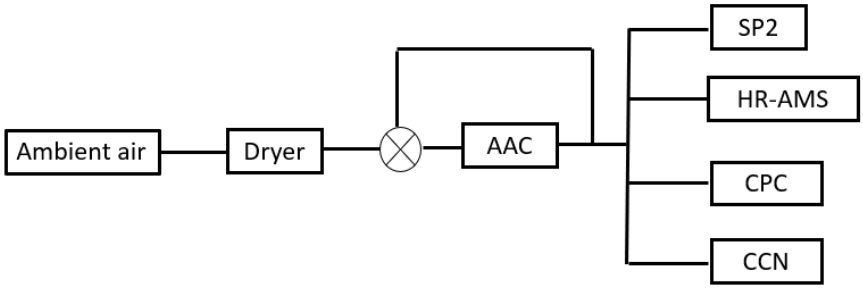

969

970 Figure 1. The schematic of the instruments set up. A timed three-way valve was
971 placed at the upstream of the AAC.

972

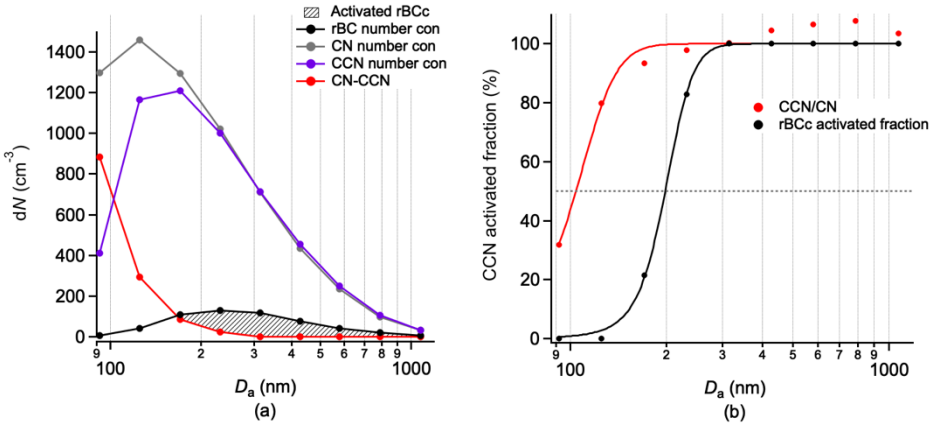

973

974 Figure 2 An example of all particles and rBCc activation, the dashed grey line in (b)
975 indicated the 50% of all particles or rBCc activated.

976

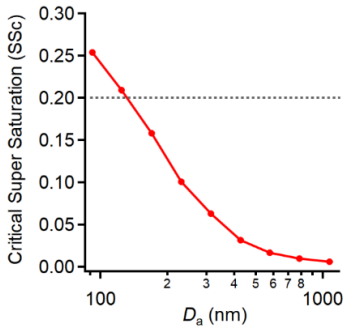

977

978 Figure 3 An example of the calculation of the size-resolved critical supersaturation
979 (SSc)

980

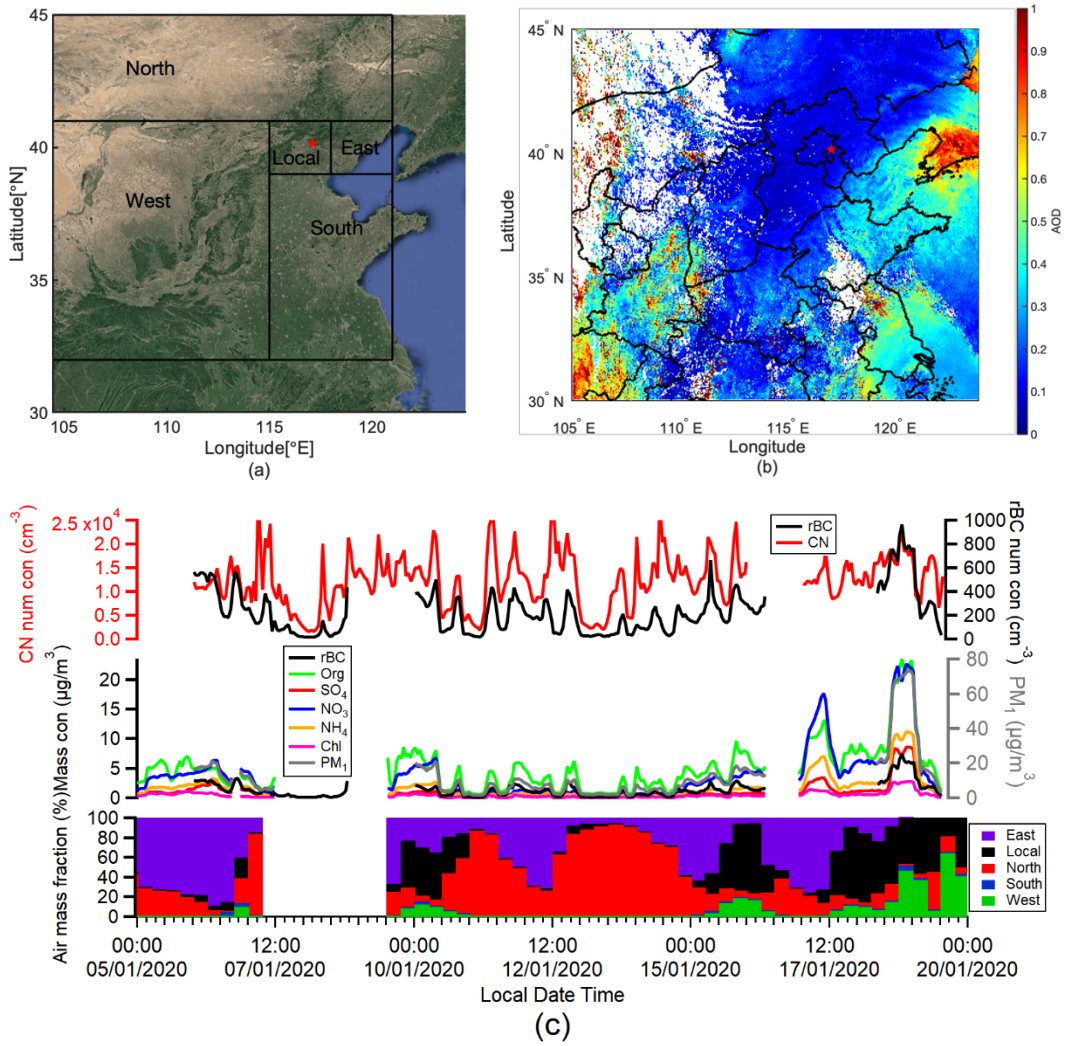

Figure 4. Overview of the experiment. (a) Location of the measurement site (marked in red pentagram) and regions classified for air mass; (b) The mean aerosol optical depth (AOD) distribution during the experiment period; (c) Aerosol mass and number concentrations and classified air mass types.

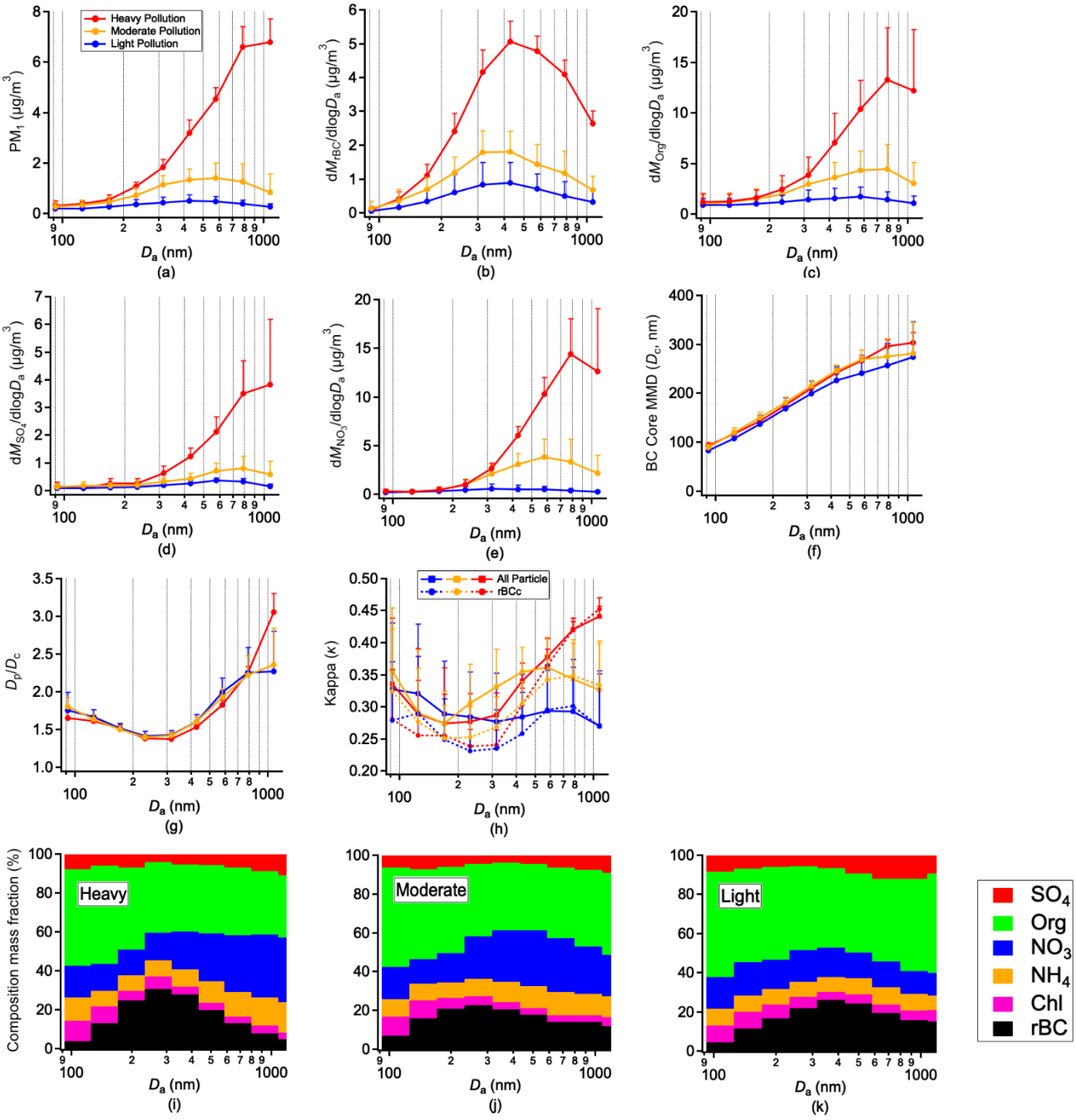

Figure 5 Size-resolved (a) PM_1 (mean ± standard deviation); (b) rBC mass concentration; (c) Org mass concentration; (d) SO_4 mass concentration; (e) NO_3 mass concentration; (f) size-resolved rBC core mass median diameter (MMD); (g) size-resolved coating thickness (D_p/D_c) of rBCc; (h) hygroscopicity parameter (κ); (i, j, k) aerosol composition mass fractions under three different pollution levels.

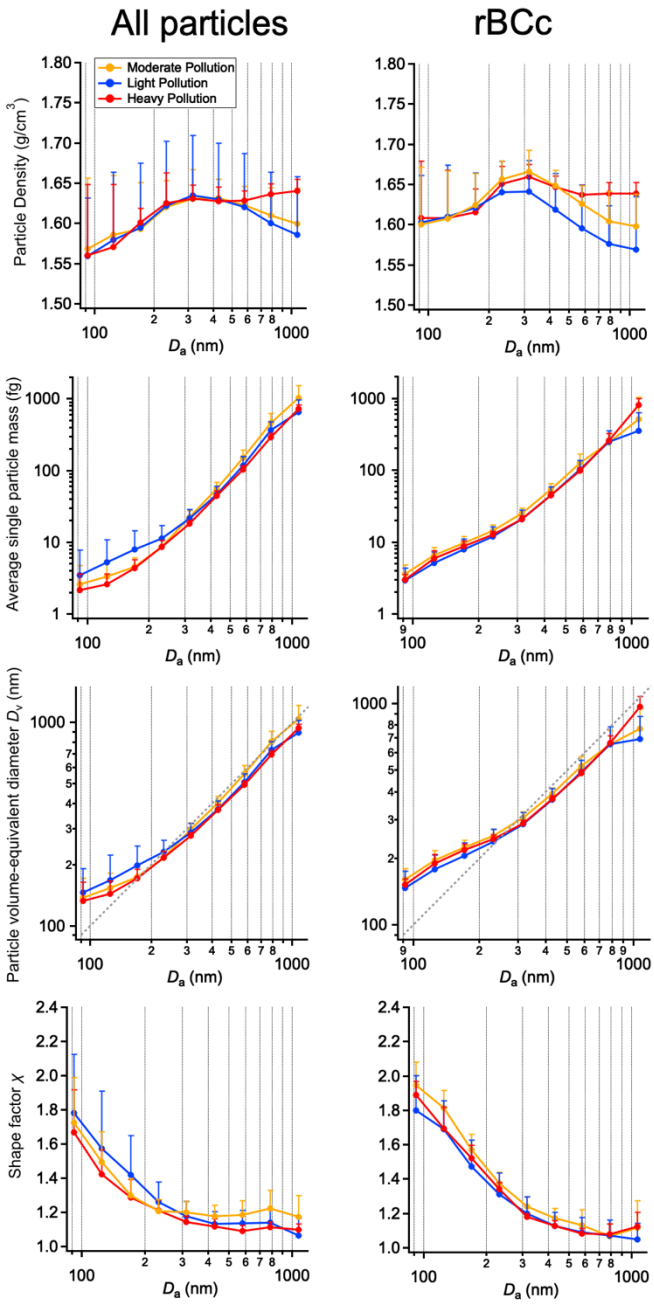

994

995 Figure 6 The particle density, average single particle mass, shape factor and volume-
996 equivalent diameter for all particles (All Particles, left) and refractory Black Carbon
997 containing particles (rBCc, right) under different pollution level.

998

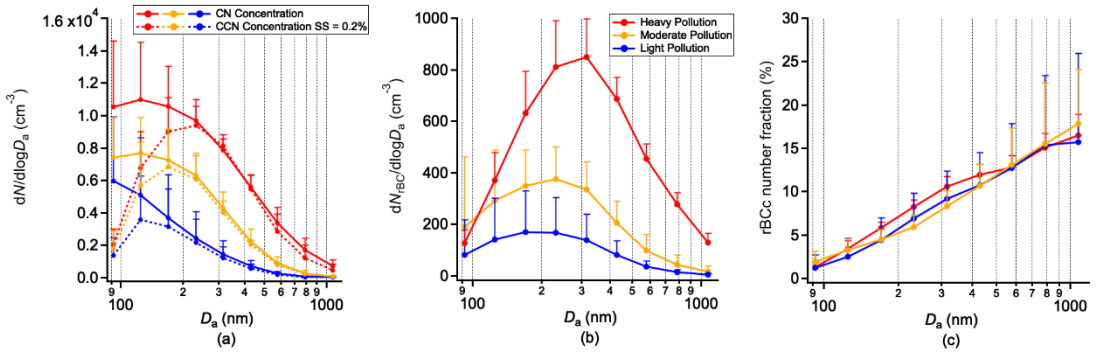

999

1000 Figure 7 Size-resolved (a) CN and CCN at SS = 0.2% number concentrations; (b) rBC

1001 number concentration; (c) rBCc number fraction.

1002

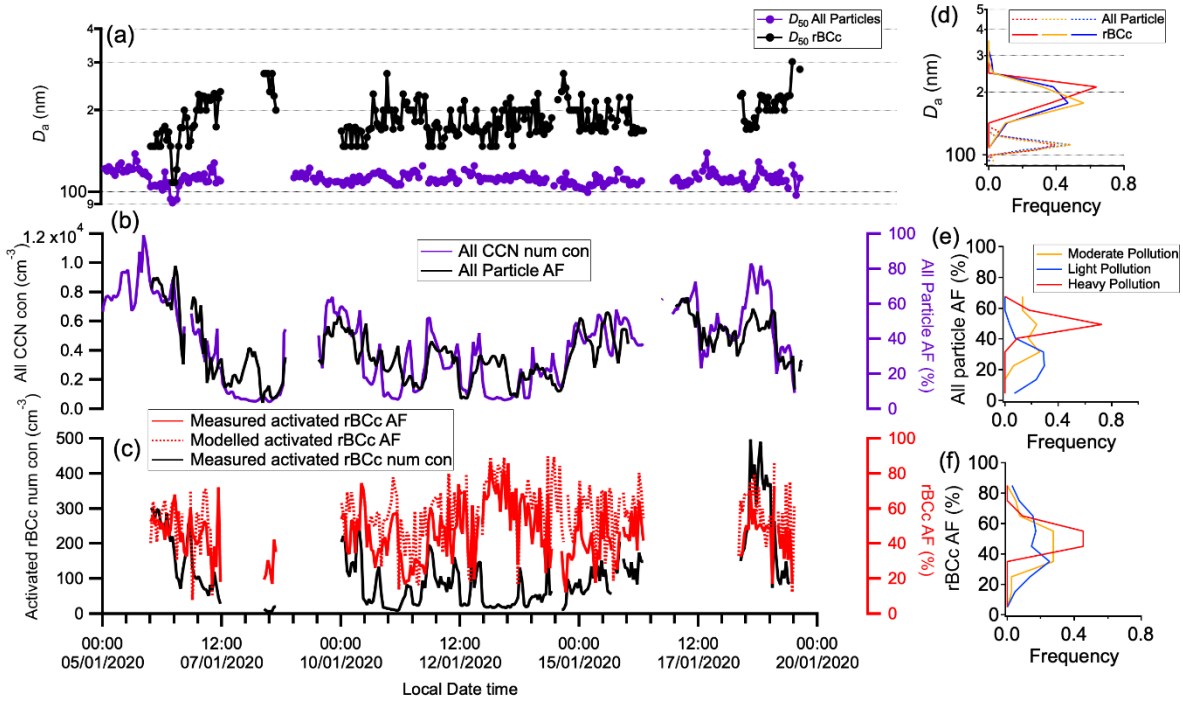

1003

1004 Figure 8 CCN activities of all particles and rBCc. (a) Time series of D_{50} for all particles

1005 and rBCc; (b) Time series of all CCN number concentrations and all particles activation

1006 fractions; (c) Time series of measured activated rBCc number concentrations, and rBCc

1007 activation fractions from two methods; (d) Frequency of D_{50} for all particle and rBCc;

1008 (e) Frequency of all particles activation fraction; (f) Frequency of measured rBCc

1009 activation fraction.

1010

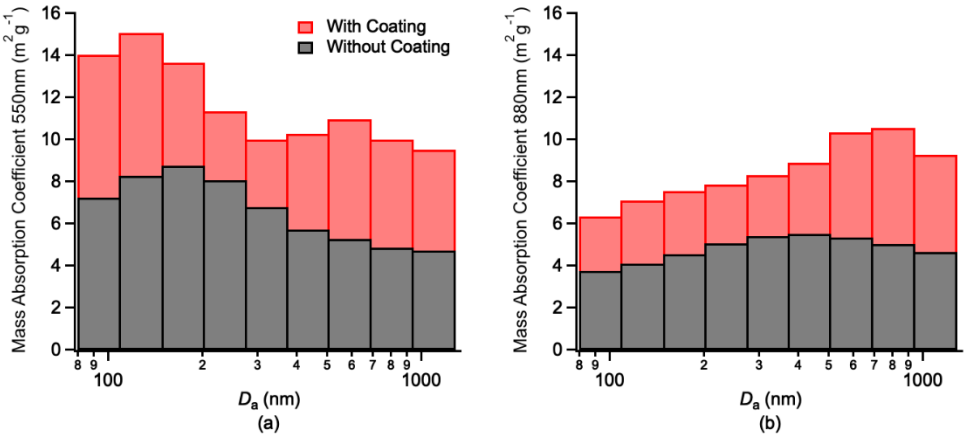

Figure 9 Mass Absorption Coefficient (MAC) at (a) 550nm (b) and 880 nm wavelength for coated and uncoated rBCc.

Appendix A Parameters used for the calculation of size-resolved shape factors

Parameter	Description	Calculation/Measurement	References
$\boldsymbol{M_{NR}}$	Mass concentration of total non-refractory compositions	Sum of AMS results	
$\boldsymbol{M_{rBC}}$	Mass concentration of rBC	SP2 measurement	
$\boldsymbol{M_{all}}$	Mass concentration of all particles	Sum of AMS and SP2 results	
$\boldsymbol{N_{total}}$	Number concentration of all particles	CPC measurement	
$\boldsymbol{V_{all}}$	Volume of all particles	$V_{all} = \frac{M_{(NH_4)_2SO_4}}{\rho_{(NH_4)_2SO_4}} + \frac{M_{NH_4NO_3}}{\rho_{NH_4NO_3}} + \frac{M_{NH_4HSO_4}}{\rho_{NH_4HSO_4}} + \frac{M_{H_2SO_4}}{\rho_{H_2SO_4}} + \frac{M_{Org}}{\rho_{Org}} + \frac{M_{rBC}}{\rho_{rBC}}$	(Gysel et al., 2007; Hu et al., 2021a)
$\boldsymbol{V_{NR}}$	Volume of non-refractory compositions	$V_{NR} = \frac{M_{(NH_4)_2SO_4}}{\rho_{(NH_4)_2SO_4}} + \frac{M_{NH_4NO_3}}{\rho_{NH_4NO_3}} + \frac{M_{NH_4HSO_4}}{\rho_{NH_4HSO_4}} + \frac{M_{H_2SO_4}}{\rho_{H_2SO_4}} + \frac{M_{Org}}{\rho_{Org}}$	(Gysel et al., 2007; Hu et al., 2021a)
$\boldsymbol{D_c}$	Mass equivalent diameter of rBC core	SP2 measurement	

$\boldsymbol{D_{p,rBCc}}$	Volume equivalent diameter of rBC-containing particle	SP2 LEO fitting method, assumed to be equal to the optical diameter	(Liu et al., 2019)
$\boldsymbol{\rho_{NR}}$	Non-refractory aerosol composition density	$\rho_{NR} = \frac{M_{NR}}{V_{NR}}$	(Hu et al., 2021a)
$\boldsymbol{\rho_{all}}$	All particles density	$\rho_{all} = \frac{M_{all}}{V_{all}}$	

1018